IJMF, Iranian Journal of Materials Forming, Vol. 3, No. 1, pp 55-64
Printed in The Islamic Republic of Iran, 2016

Experimental Investigation on Stretchability of an Austentic Stainless Steel 316L

S. Kathiravan, A. Naveen Sait* and M. Ravichandran

Department of Mechanical Engineering, Chendhuran College of Engineering and Technology, Pudukkottai -622 507, Tamil Nadu, India

Abstract: Forming limit diagram (FLD) is composed of negative and positive minor strain with respect to major strain, which occurs at directional zero strain with the critical thickness of sheet metal. The negative minor strain region of FLD is predicted by localized necking. However, there is no directional zero strain in the positive minor region of FLD which could be predicted with the help of Marcinaik-Kuczynski assumption. The present work aims to determine the stretchability in terms of limiting strain of Austentic stainless steel 316L using M K analysis and hemi spherical dome stretching. Strain hardening exponent was derived from uni axial tensile test of Austentic stainless steel 316L. C++ program was developed to predict the theoretical FLD and the results were compared with the experimental value. The limiting strain of material is found as 0.4 in the experimental and Marcinaik - Kuczynski analysis. Fractography shows the large amount of cleavage fracture and becomes an evidence for cleavage initiating due to other inclusions.

Keywords: Forming Limit Diagram (FLD), Marcinaik-Kuczynski analysis, Simulation in C++, Sheet Metal.

1. Introduction

Austenitic stainless steels are widely used in many fields of industry because of their excellent mechanical and functional properties, such as high ductility and high strength, as well as excellent corrosion and heat resistances [1]. The demand for stainless steels has been increasing in various areas such as electronics, automotive and building industries due to their high corrosion resistance, high mechanical strength and good surface appearance. Simultaneously, the development of advanced forming processes using stainless steel sheet are in progress because the formability of stainless steels under various process conditions has not been thoroughly investigated [2]. The forming-limit curve or FLC is one of the best tools available to metallurgical engineers in order to assess a particular steel sheet's ability to be drawn or stretched. The FLC is either a curve or band of finite width that is plotted in the in-plane strain space of a material sheet. Extending between uniaxial and balanced biaxial-tension stress states, the FLC separates the region of uniform sheet deformation from the region of slightly greater deformation, where the sheet will likely develop a local deformation instability or neck. The concept of the FLC is most applicable to the stretching process, in which the boundaries of the sheet being formed are fixed [3]. Forming limit diagrams (FLDs), first proposed by Keeler and Goodwin, has proved to be a useful tool to represent conditions for the onset of necking and evaluate formability of sheet metals [4]. The forming limit diagram (FLD) is used to record estimates of the strains experienced by a particular material in one or more forming process [5]. Korhonen et al studied forming and fracture limits of austenitic stainless steel sheets and the fracture limit strains calculated using the modified Rice–Tracey criterion [6]. A new methodology was proposed by Mitukiewicz et al to obtain forming limit diagrams of sheet materials using

Received by the editors February 30, 2016; Revised April 17, 2016 and Accepted April 19, 2016.
*Corresponding author (naveensait@yahoo.co.in)

gas blow forming process at elevated temperatures. Tension–tension side of the forming FLD is achieved by using circular as well as elliptical dies of different aspect ratios [7]. A new methodology was introduced to compare the experimental FLDs for three different grades of low carbon steels and an aluminum alloy. The calculation of FLDs using the predicted anisotropic FLD, assuming Hill48 yield criterion was illustrated for one of the materials [8]. Sansot Panich et al studied the experimental and numerical analyses of Forming Limit Diagram and Forming Limit Stress Diagram for two Advanced High Strength Steel sheets of grade DP780 and TRIP780 [9]. Zhou et al carried out experimental work on FE simulation of elliptical bulge forming of AZ31 automotive magnesium [10]. Assempour et al presented a methodology for prediction of the forming limit stress diagram based on the Marciniak and Kuczynski model. For the calculation of sheet metal limiting strains and stresses, a numerical approach using the Modified Newton–Raphson with globally convergence method was used [11]. The forming behaviour of type 304 stainless steel sheet was investigated by Makkouk et al and characterized in uniaxial tension tests, and the forming limits at necking and at fracture was determined using the Marciniak punch test [12].

Based on the above literature review, the present work aims to find the stretchability in terms of limiting strain of austentic stainless steel 316L and to determie the experimental limit strain. Moreover, it has to be checked with M K simulation using the Hollomon equation derived from tensile test. The role of inhomogeneity in the forming limit diagram is to be analyzed and the fracture analysis of stretched material was carried out.

2. Experimental Details

2.1. Material

The material used for this investigation is AISI type 316L stainless steel and the size of the material is 2000 X 1000 X 1.6 mm. The composition of 316L stainless steel is given in Table 1.

2.2. Tensile test

The dimensions of the tensile test specimens are shown in Fig.1 and it was cut from the sheet metal by wire electric discharge machine. The conventional tensile test was carried out in a universal tensile testing machine (Hung Ta 2402) at strain rate of 0.486 mm/min at room temperature. The data from the tests were digitally acquired as load – cross head displacement. The load –displacement values were converted to engineering stress – engineering strain values using the formula $s= P/A_0$ and $e = \Delta l/ l_0$ where s is the engineering stress, P is the load, A_0 is the initial cross sectional area, e is the engineering strain, Δl is the cross head displacement and l_0 is the length of the parallel section of the tensile specimen. The 0.2% proof stress was determined by the usual offset method. The total elongation was measured by placing the fractured ends together and measuring the distance between the scribed gage marks. To obtain the true stress - true strain from the engineering stress – engineering strain data, the slope K' of the initial portion (linear) of the curve was determined. The engineering true stress – true strain for all points was determined using the formulae given below [13].

$$\sigma = \boldsymbol{s}(1+\boldsymbol{e}) \tag{1}$$

$$\varepsilon = \ln(1+(\boldsymbol{e}-\frac{\boldsymbol{s}}{\boldsymbol{K'}})) \tag{2}$$

The true stress – true strain data obtained above was fitted to Hollomon, Ludwik and Swift constitutive equations. The actual constitutive equations are reproduced below.

Hollomon equation $\sigma = K\varepsilon^{n}$ (3)

Ludwik $\sigma = \sigma_0 + K''\varepsilon^{n'}$ (4)

Swift Equation $\sigma = K'''(\varepsilon + \varepsilon_0)^{n''}$ (5)

where K, K'', K''', n, n' and n'' are constant. The Ludwik constitutive equation is chosen to determine theoretical limiting strain of material.

2.3. Normal anisotropy

Normal anisotropy R of the material was determined [13] as per ASTM E 517 standards on the tensile specimens by making gage marks using the Vickers indenter with 100 kg load along the length and the width of the specimen followed by plastic deformation to about 15% strain. The gage lengths were measured before and after the deformation using Nikon Microscope with a precision of ±1μm. Assuming volume constancy, the R-value is derived (given in ASTM E 517) to be:

$$R = \frac{\ln(w_0 / w_f)}{\ln(l_f w_f / l_0 w_0)} \tag{6}$$

2.4. M K simulation

Forming Limit Diagrams were simulated for positive minor strains using the Marciniak – Kuczynski method outlined earlier. The force balance across the imperfection is

$$\sigma_{1a} t_a = \sigma_{1b} t_b \tag{7}$$

while the strain compatibility between the imperfection and the bulk is given by

$$d\varepsilon_{2a} = d\varepsilon_{2b} \tag{8}$$

where subscripts a and b refer to the bulk and imperfection respectively, subscripts 1, 2, 3 are to the appropriate principal values and t is the thickness of the material. Assuming the Hollomon equation to be valid, and using the formulae for equivalent stress for the Von Mises yield criterion, the following equation is obtained.

$$\left(\frac{\sigma_{1a}}{\bar{\sigma}_a}\right)(\varepsilon_a)^n \exp(\varepsilon_{3a}) = f\left(\frac{\sigma_{1b}}{\bar{\sigma}_b}\right)(\varepsilon_b)^n \exp(\varepsilon_{3b}) \tag{9}$$

where

$\bar{\sigma}$ is the equivalent stress and $f = \frac{t_{0b}}{t_{0a}}$ is the initial imperfection parameter.

The subscript 0 refers to the initial state (in this case the initial thicknesses of the two regions). The strain ratios in region ‘a’ is first fixed for the simulation. Strains are incremented in ‘a’ and the resulting strains and strain ratio in region ‘b’ is computed by making equal to the right side of the above equation to the left side. A convergence criterion of 10^{-6} was used. The iterations are repeated for a further increment in the ratio of equivalent strain increments in ‘a’ to the resulting equivalent strain increment in ‘b’ which exceeds to 5. At this point, it is assumed that the localized neck has formed and the principal strains are considered to be limiting strains for the specific strain ratios. The computation is repeated for various strain ratios from 1 to near 0 to generate the forming limit diagram.

Table 1. Composition of SS316L

SS316L	C	Mn	Si	P	S	Cr	Mo	Ni	N
Min	-	-	-	-	-	16.0	2.00	10.0	-
Max	0.03	2.0	0.75	0.045	0.03	18.0	3.00	14.0	0.10

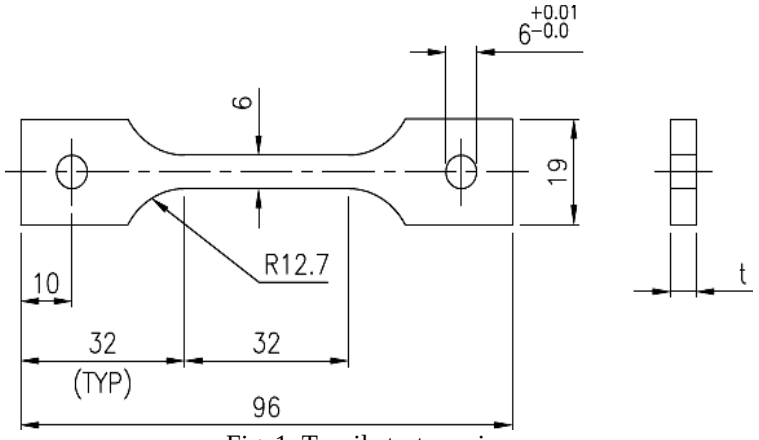

Fig. 1. Tensile test specimen

2.5. Hemi spherical dome stretching

In this study the FLD was determined by hemispherical punch stretching [14]. The specimens were laser gridded with 5 mm diameter circles in the portion that has to be stretched. Stretching of the blanks was carried out by hemispherical punch stretching till the sheet failed by necking or fracture. The measurements of the distorted grid were used to determine the principal strains. The stretching operation was done in a refurbished MTS Metal forming Test system with controllers supplied by M/s BiSS, Bangalore. The diameter of the punch was 100 mm and clamping of the sheet metal was done by means of a blank holder with a force of 550 kN. Stretching was done by displacing the punch at velocity of 30 mm/minute till the specimen failed by necking or fracture. The blank holding force was adequate to prevent drawing of the specimen and to ensure pure stretching by the punch. The details of specification of hemi spherical dome stretching are given in Table 2.

Table 2. Specification of Hemi Spherical Dome Stretching

Sl. No.	Parameters	Values
1	Size	All
2	Blank-Holding force	550 kN
3	Blank holding force Rate	50/Sec
4	Punch Stroke	70 mm
5	Strain Rate	30 mm/min
6	Pre-Load	3kN@10/min
7	Load Termination	10% in drop force

The dimensions of the blank varied from 200 mm x 200 mm to 200 mm x 25mm to obtain positive and negative minor strain. Limiting strains was obtained for the square sheets in the positive minor strain region. To determine the negative minor strains, the width of the sheets selected as 125, 100, 75, 50 and 25 mm. Teflon, grease and combinations of both were used as lubricants between the punch and the sheet to vary the failure points on the square specimens from the regions close to equi-bi-axial stretching.

During the stretching, the circles become ellipses along constant strain ratios. The major and minor diameters of the ellipses were measured using a three dimensional co-ordinate measuring machine. The measured dimensions were used to calculate principal engineering strains using the formulae $\boldsymbol{e}_1 = \dfrac{\boldsymbol{D}_{\text{major}} - 5}{5}$ and $\boldsymbol{e}_1 = \dfrac{\boldsymbol{D}_{\text{minor}} - 5}{5}$. The forming limit diagram was then plotted as the line was

separating the 'safe' strains and the 'failed' strains. In the FLD, no 'failed' points lies below the line while safe points can lie above the line.

3. Results and Discussion

3.1. Uniaxial tensile tests

Figure 2 shows the engineering stress – strain curve of the tensile tests specimens drawn for the rolling and transverse direction. The true stress- true strain curve obtained from the test is provided in Fig. 3. The 0.2% proof stress, ultimate tensile strength, elongation and percentage elongation are provided in table 3. It is clear from the data that the total elongation is high along the rolling directions and less in the transverse direction. Since the inclusions are all along the rolling direction, the increased percentage elongation was observed. Another feature of the results is the small post uniform elongation. Austenitic stainless steels of this type would be expected to show much larger post uniform elongation. From the measured R-values, it was identified that the material is isotropic. Figure 4 indicates the plastic true stress-strain curves along the rolling and transverse direction. Table 4 lists the best fits for the Hollomon, Ludwik and Swift constitutive equations. From the plastic true stress- strain curves the strain hardening exponent and strength coefficient were determined [15].

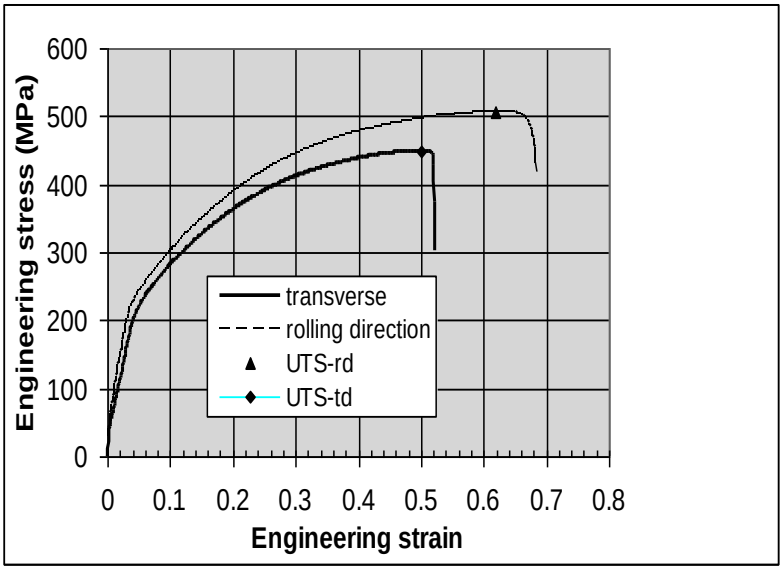

Fig. 2. Engineering stress - strain curve.

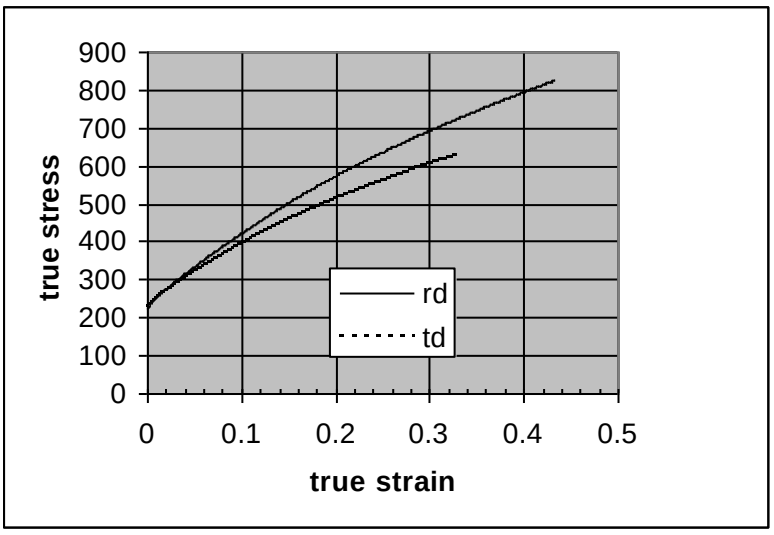

Fig. 3. True stress - strain curve.

Table 3. Tensile properties.

Property	Rolling Direction	Transverse Direction
Yield Stress	214MPa	223 MPa
Ultimate Stress	507MPa	453 MPa
Elongation	42.08 mm	39.06 mm
Gauge length	28.02mm	28.02 mm
Percentage of elongation	50.17	32.2 mm

Table 4. Best fits for the Hollomon, Ludwik and Swift constitutive equations.

Constitutive Equation	Rolling Direction	Transverse Direction
$\sigma = K\varepsilon^n$	$\sigma= 805.6\ \varepsilon^{0.33226}$	$\sigma= 1134\varepsilon^{.409}$
$\sigma = \sigma_y+K\varepsilon^n$	$\sigma= 211+1021\varepsilon^{0.496}$	$\sigma= 208+912\varepsilon^{.690}$
$\sigma = K(\varepsilon+ \varepsilon_0)^n$	$\sigma= 1253(\ \varepsilon+0.046)^{0.56}$	$\sigma= 1136(\varepsilon+ 0.0385)^{0.705}$

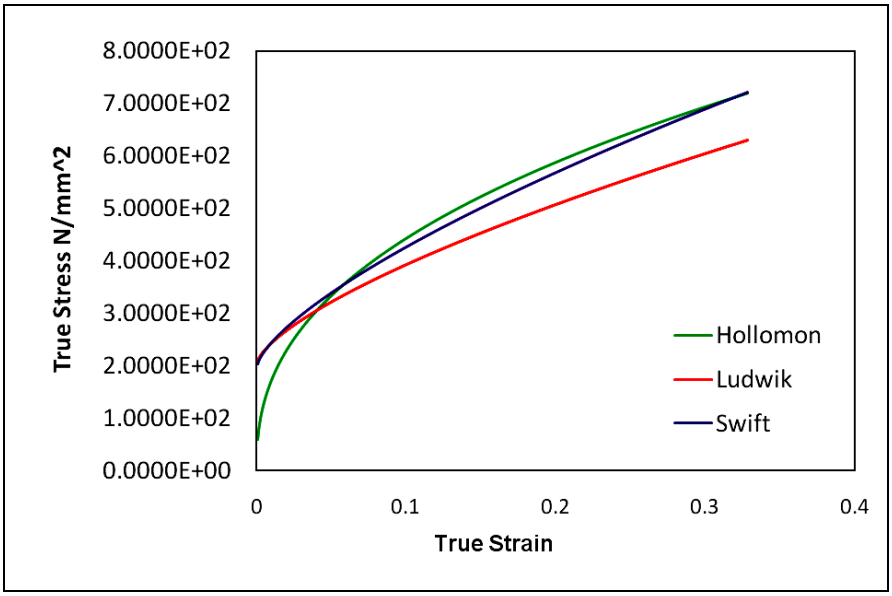

Fig. 4. Fitting curves of TD.

3.2. Forming limit diagram

A characteristic of this FLD is that it is almost flat unlike the V shape with a minimum elongation at plane strain as shown in Fig. 5. The ductility is expected to be close to the exponents in the Ludwik and Swift equations at plane strain. It was observed that the failure was rapid and brittle. The characteristic alignment of the neck at an angle to the maximum principal stress direction was not observed. Instead the fracture took place normal to the major principal direction. All these observations indicate a high inclusion in the material and limiting strain value is observed from FLD as 0.4, observed from the Fig 5. In Fig.6, limiting strain of material is 0.4 under the inhomogeneity level of 0.98 which almost equals the experimental result as shown in Fig. 5.

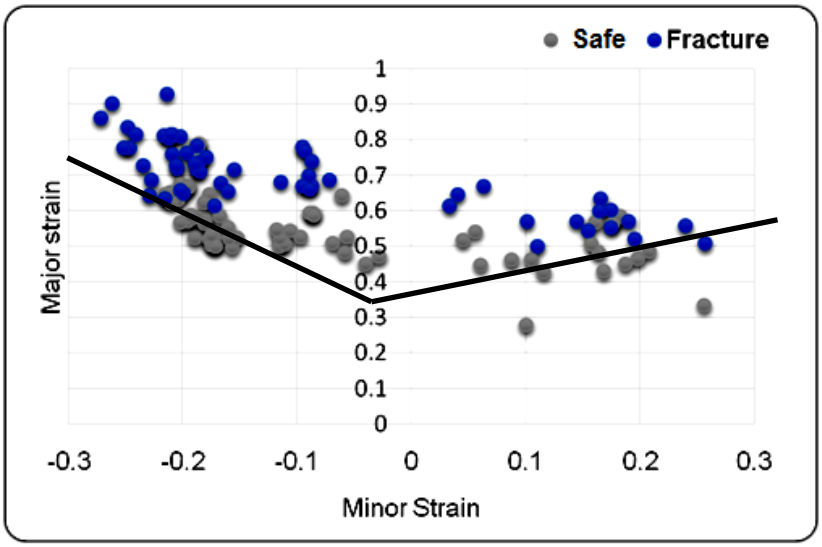

Fig. 5. Forming limit diagram of austentic stainless steel.

3.3. M K simulation

The result of M K simulation of limiting strain under different inhomogeneity like 0.998, 0.99, and 0.98 are shown in Fig. 6. Quite clearly the M-K simulations do not fit the experimental data. In general, increasing the strain hardening exponent would increase the plane strain values. Decreasing inhomogeneity value makes the FLD more flat but also lowers the plane strain limits. All this seems to indicate that fracture and not localised necking is occurred. Moreover, it was observed that these are the factors of controlling the FLD. As like experimental result, the limiting strain of material is derived as 0.4 where inhomogeneity is equal to 0.98 and it is illustrated in Fig 6.

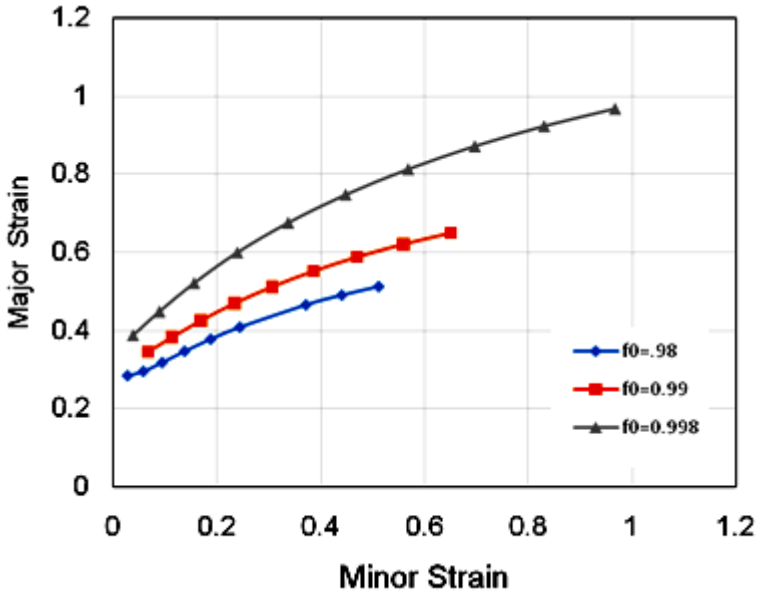

Fig. 6. M K simulation of limiting strain.

3.4. Fractography

The fracture surfaces of specimens that failed at positive minor strain, plane strain and negative minor strain were observed using a Scanning Electron Microscope. Fracture surface of specimen (200 X 25 mm) appears to be layered. From Fig.7 (a-d), though dimples are observed, larger portions of cleavages are also evident. No changes were observed for the specimens that failed under plane strain and biaxial tension. From some of the fractographs, it is apparent that brittle fracture initiated because of the inclusion. Figure

8a shows optical micrograph of polished and unetched specimens in the plane of the sheet and Fig. 8b shows it in the x-z plane of the sheet. The inclusions are clearly observed along the rolling direction, which lead difference in elongation in rolling direction as well as in transverse one even though the material is isotropic. The fractographs and optical micrographs confirm the high inclusion content in the material inhibit the good stretchability.

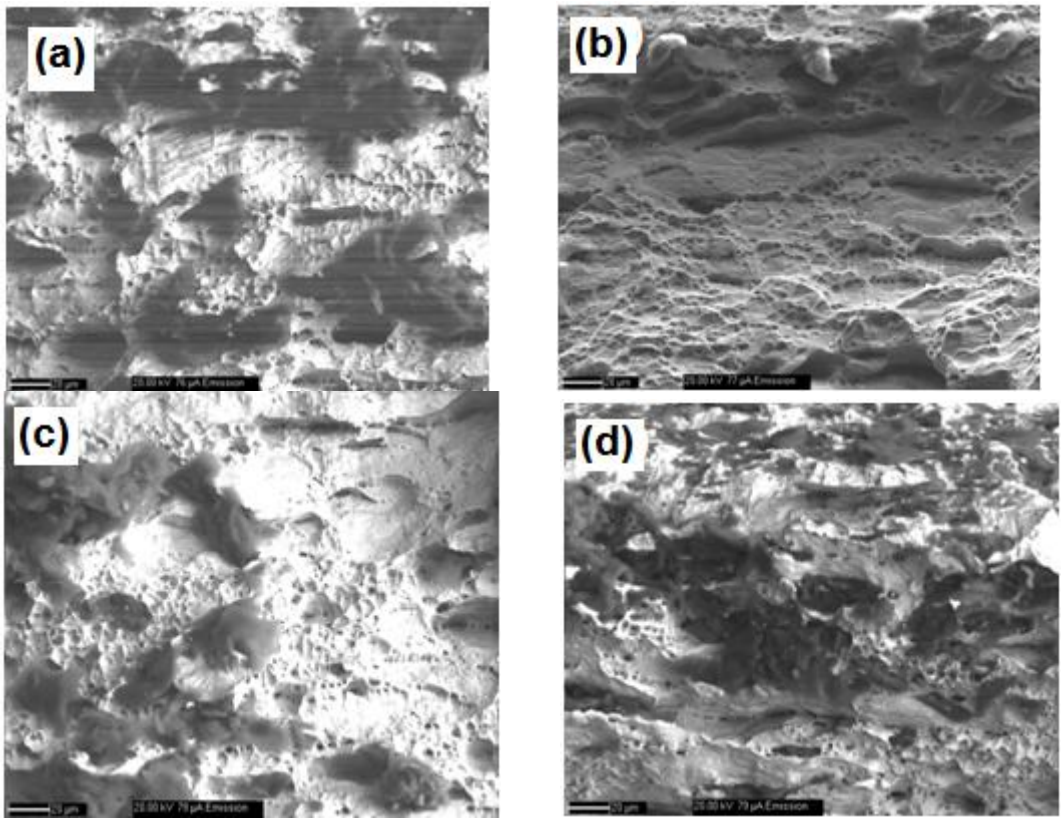

Fig. 7. SEM images of fracture surfaces (a) failed at positive minor strain region, (b) failed at positive minor strain region (higher magnification), (c) failed at negative minor strain region (sample 1), (d) failed at negative minor strain region (sample 2).

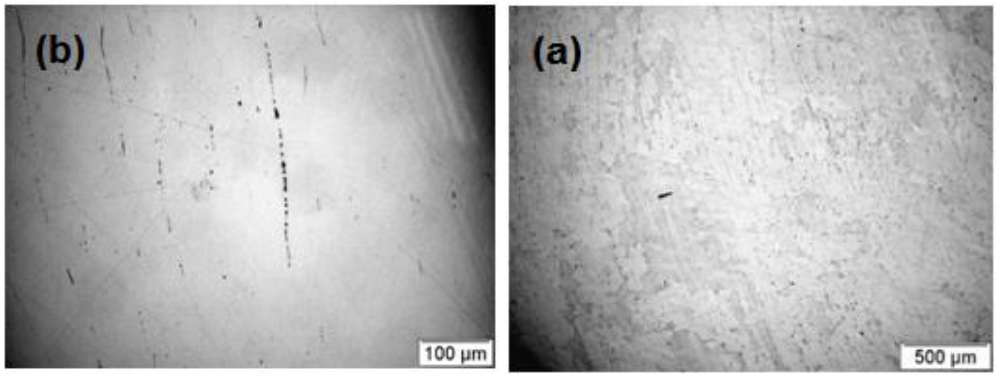

Fig. 8. Optical micrograph of polished specimen (a) in the X-Y plane of the sheet, (b) in the Y-Z plane of the sheet.

4. Conclusion

The following conclusions are drawn from the above work,

- Forming limit diagram of type AISI316L austentic stainless steel has been determined experimentally by hemispherical punch stretching. The stretchability was found to be poorer than the high strain hardening exponents obtained from the uniaxial tensile tests.

- The limiting strain of material is found as 0.4 in experimental and Marcinaik - Kuczynski analysis.
- Fractography shows the large amount of cleavage fracture and is an evidence for cleavage initiating from other inclusions. The reason for the poor strechability of the material is the large amount of inclusions of oxides.

5. References

[1] E. Ishimaru, H. and Hamasaki, F. Yoshida, Deformation-induced martensitic transformation and workhardening of type 304 stainless steel sheet during draw-bending, *Procedia Engineering*, 81 (2014) 921 – 926.

[2] H. JongBong, F. Barlat, D. ChanAhn, H.Y. Kim and M.G. Leen, Formability of austenitic and ferritic stainless steels at warm forming temperature, *International Journal of Mechanical Sciences*, 75 (2013) 94–109.

[3] G. Charca Ramos, M. Stout, R.E. Bolmaro, J.W. Signorelli, M. Serenelli, M.A. Bertinetti and P. Turner, Study of a drawing-quality sheet steel. II: Forming-limit curves by experiments and micromechanical simulations, *International Journal of Solids and Structures*, 47 (2010) 2294–2299.

[4] P. Dasappa, K. Inal and R. Mishra, The effects of anisotropic yield functions and their material parameters on prediction of forming limit diagrams, *International Journal of Solids and Structures*, 49 (2012) 3528–3550.

[5] J. M. Allwood and D. R. Shouler, Generalised forming limit diagrams showing increased forming limits with non-planar stress states, *International Journal of Plasticity*, 25 (2009) 1207–1230.

[6] A.S. Korhonen and T. Manninen, Forming and fracture limits of austenitic stainless steel sheets, *Materials Science and Engineering A*, 488 (2008) 157–166.

[7] G. Mitukiewicz, K. Anantheshwara, G. Zhou, R.K. Mishra and M.K. Jain, A new method of determining forming limit diagram for sheetmaterials by gas blow forming, *Journal of Materials Processing Technology*, 214 (2014) 2960–2970.

[8] K. Hariharan, N.T. Nguyen, F. Barlat, M.G. Lee and J.H. Kim, A pragmatic approach to accommodate in-plane anisotropy in forming limit diagrams, *Mechanics Research Communications*, 62 (2014) 5–17.

[9] S. Panich, F. Barlat, V. Uthaisangsuk, S. Suranuntchai and S. Jirathearanat, Experimental and theoretical formability analysis using strain and stress based forming limit diagram for advanced high strength steels, *Materials and Design*, 51 (2013) 756–766.

[10] G. Zhou, K. Ananthaeswara, G. Mitukiewicz, D. Li, R.K. Mishra and M.K. Jain, FE simulations of gas blow forming and prediction of forming limitdiagram of AZ31 magnesium sheet, *Journal of Materials Processing Technology*, 218 (2015) 12–22.

[11] Assempour, R. Hashemi, K. Abrinia, M. Ganjiani and E. Masoumi, A methodology for prediction of forming limit stress diagrams considering the strain path effect, *Computational Materials Science*, 45 (2009) 195–204.

[12] R. Makkouk, N. Bourgeois, J. Serri, B. Bolle, M. Martiny, M. Teaca and G. Ferron, Experimental and theoretical analysis of the limits to ductility of type 304 stainless steel sheet, *European Journal of Mechanics A/Solids*, 27 (2008) 181–194.

[13] K.S. Chan, D.A. Koss and A.K. Ghosh, Localised necking of sheet at negative minor strain, *Metallurgical Transactions A*, 15 (1984) 323-329.

[14] S. Stören and J.R. Rice, Localized necking in thin sheets, *Journal of the Mechanics and Physics of Solids*, 23 (1975) 421-441.

[15] M. Ravichandran, A. Naveen Sait and V. Anandakrishnan, Densification and deformation studies on powder metallurgy Al–TiO_2–Gr composite during cold upsetting, *Journal of Materials Research*, 29 (2014) 1480-1487.

مطالعه آزمایشگاهی قابلیت کشش پذیری فولاد زنگ نزن آستنیتی 316L

اس. کتیراوان، آ. نوین سایت، ام. راویچاندران
بخش مهندسی مکانیک، دانشکده فنی و مهندسی چندهوران، پادوکوتای، تامیل نادو، هند.

چکیده: منحنی حد شکل دهی (FLD) متشکل از کرنش مثبت و منفی فرعی نسبت به کرنش اصلی می باشد. این منحنی در کرنش صفر محوری و در راستای ضخامت بحرانی ورق فلزی بدست می آید. ناحیه کرنش منفی فرعی منحنی FLD از طریق گلویی شدن موضعی پیش بینی می شود. از آنجا که در ناحیه کرنش مثبت فرعی، کرنش صفر محوری وجود ندارد، بنابراین این منحنی به کمک فرض مارسنیاک-کوزانسکی پیش بینی می شود. در پژوهش حاضر، تلاش شده است که مقدار کشیدگی بر حسب کرنش حدی فولاد زنگ نزن آستنیتی 316L با استفاده از آنالیز MK و کشیدگی گنبد نیمه کروی تعیین شود. نمای کارسختی فولاد زنگ نزن آستنیتی 316L به کمک آزمون کشش بدست آمد. برای پیش بینی منحنی FLD از برنامه C++ استفاده و نتایج تئوری با نتایج آزمایشگاهی مقایسه شد. کرنش حدی ماده به کمک نتایج آزمایشگاهی و آنالیز MK به اندازه 0.4 اندازه گیری شد. نتایج سطح شکست نشان داد که به دلیل حضور آخالها شکست عمدتا از نوع گسیختگی است .

کلمات کلیدی: نمودار حد شکل دهی (FLD)، آنالیز مارسنیاک-کوزانسکی، شبیه سازی با استفاده از برنامه C++.